Renormalized Phase Dynamics in Oscillatory Media

Naofumi Tsukamoto,[1,*] Hirokazu Fujisaka,[1,†] and Katsuya Ouchi[2]

[1]*Department of Applied Analysis and Complex Dynamical Systems, Graduate School of Informatics, Kyoto University, Kyoto 606-8501, Japan*

[2]*Kobe Design University, Kobe 651-2196, Japan*

(Received 27 December 2006; published 27 September 2007)

Based on the complex Ginzburg-Landau equation (CGLE), a new mapping model of oscillatory media is proposed. The present dynamics is fully determined by an effective phase field renormalized by amplitude. The model exhibits phase turbulence, amplitude turbulence, and a frozen state reported in the CGLE. In addition, we find a state in which the phase and amplitude have spiral structures with opposite rotational directions. This state is found to be observed also in the CGLE. Thus, one concludes that the behaviors observed in the CGLE can be described by only the phase dynamics appropriately constructed.

DOI: 10.1103/PhysRevLett.99.134102 PACS numbers: 05.45.−a, 82.40.Bj

Various spatiotemporal patterns are observed in nonequilibrium systems, such as fluid systems, chemical reaction, and nonlinear optics [1]. Such dynamics in spatially extended systems are often described by nonlinear partial differential equations. The complex Ginzburg-Landau equation (CGLE) is one of the most-studied nonlinear partial differential equations. The CGLE is a universal equation which describes slow spatiotemporal variation near a supercritical Hopf bifurcation [2] and exhibits a rich variety of dynamical behaviors [3–5] in spite of its simple form

$$\dot{A}(\boldsymbol{r}, t) = A - (1 + ic_2)|A|^2 A + D(1 + ic_1)\nabla^2 A, \quad (1)$$

where c_1, c_2, and $D(>0)$ are real parameters and A is the complex order parameter. Almost 20 years ago, for efficiency of numerical simulations, some partial differential equations were approximated by mapping models [6,7]. Mapping models of the CGLE have been also obtained and investigated as an approximation [3,8–13].

In this Letter, we consider a mapping model of the CGLE in order to extract the essential natures of the CGLE. We use the mapping model constructed by the method proposed in Refs. [12,13], which is similar to those in Refs. [3,8–11]. There are two steps to obtain mapping models: (i) splitting the time evolution of the CGLE into two parts and (ii) recombining them. One of the divided two parts is a local part which consists of the first two terms in the right-hand side of Eq. (1), and the other is a nonlocal part which is the spatial coupling term in Eq. (1). The time evolution of each part can be solved analytically as shown below.

The time evolution of the local part is described by the Stuart-Landau equation $\dot{A} = A - (1 + ic_2)|A|^2 A$, which is obtained by omitting the spatially coupling term in Eq. (1). Integrating the Stuart-Landau equation over time width τ and setting $\psi(t) = e^{ic_2 t} A(t)$, we obtain

$$\psi(t + \tau) = F_\tau(\psi(t)), \quad (2)$$

where $F_\tau(\psi) = \psi\{(1 - e^{-2\tau})|\psi|^2 + e^{-2\tau}\}^{-(1+ic_2)/2}$. The time evolution of the nonlocal part is described by the complex diffusion equation $\dot{\psi} = D(1 + ic_1)\nabla^2\psi$, which is obtained by omitting the local parts in the right-hand side of Eq. (1). Integrating the equation over time width τ, we have

$$\psi(\boldsymbol{r}, t + \tau) = \mathcal{L}_{D\tau}\psi(\boldsymbol{r}, t), \quad (3)$$

where $\mathcal{L}_{D\tau}$ is the linear operator defined by $\mathcal{L}_{D\tau} f(\boldsymbol{r}) = \int K_{D\tau}(\boldsymbol{r} - \boldsymbol{r}') f(\boldsymbol{r}') d\boldsymbol{r}'$. Here $K_{D\tau}(\boldsymbol{r}) = \{4\pi D\tau(1 + ic_1)\}^{-d/2} e^{-|\boldsymbol{r}|^2/4D\tau(1+ic_1)}$, and d is the spatial dimensionality. Recombining the divided time evolutions, we obtain the mapping model

$$\psi_{n+1}(\boldsymbol{r}) = \mathcal{L}_{D\tau} F_\tau(\psi_n(\boldsymbol{r})). \quad (4)$$

This equation is a model based on the CGLE with a control parameter τ and coincides with Eq. (1) in the limit $\tau \to 0$. Therefore, Eq. (4) for small τ is expected to show approximately the dynamics in the CGLE. Actually, the spatiotemporal dynamics in the CGLE have been investigated by using mapping models similar to Eq. (4) as an approximation [3,8–11].

In this Letter, we take the opposite limit $\tau \to \infty$ by keeping $D\tau = 1$ fixed. In this limit, the local map $F_\tau(\psi)$ reduces to

$$F(\psi) \equiv F_\infty(\psi) = \begin{cases} \psi|\psi|^{-(1+ic_2)} & (\psi \neq 0), \\ 0 & (\psi = 0), \end{cases} \quad (5)$$

which maps an arbitrary state ψ onto either a state on the limit cycle ($|\psi| = 1$) or the unstable fixed point ($\psi = 0$) of the Stuart-Landau equation. Thus, the limit $\tau \to \infty$ removes the relaxation process to the limit cycle. By setting $\mathcal{L} \equiv \mathcal{L}_{D\tau=1} = e^{(1+ic_1)\nabla^2}$, the above procedure leads to the complex Ginzburg-Landau map (CGLM)

$$\psi_{n+1}(\boldsymbol{r}) = \mathcal{L} F(\psi_n(\boldsymbol{r})). \quad (6)$$

We will show that the CGLM (6) exhibits the spatiotem-

poral behaviors reported in the CGLE and discuss the essence of the CGLE dynamics.

It should be noted that the limit $\tau \to \infty$ allows us to renormalize the amplitude component into the phase variable as follows. Introducing the renormalized phase variable $\theta_n = \arg\psi_n - c_2 \log|\psi_n|$ for $\psi_n \neq 0$, we define the phase field with the phase singular point as $z_n(\boldsymbol{r}) \equiv F(\psi_n(\boldsymbol{r}))$, that is, $z_n(\boldsymbol{r}) = e^{i\theta_n(\boldsymbol{r})}$ for $\psi_n(\boldsymbol{r}) \neq 0$ and $z_n(\boldsymbol{r}) = 0$ for $\psi_n(\boldsymbol{r}) = 0$. Here $z_n = 0$ represents the phase singular point, and θ_n describes an isochron of the Stuart-Landau equation. Equation (6) can be written as $\psi_{n+1}(\boldsymbol{r}) = \mathcal{L} z_n(\boldsymbol{r})$, which indicates that the time evolution of ψ_n is determined by z_n. In addition, we obtain the mapping system of the phase field with the phase singular point as

$$z_{n+1}(\boldsymbol{r}) = F(\mathcal{L} z_n(\boldsymbol{r})), \tag{7}$$

which is the phase description of the CGLM. Because there is no approximation through the derivation of Eq. (7) from Eq. (6), this phase description is valid even when the CGLM exhibits a state in which the amplitude plays an important role in dynamics. In the case that there is no phase singular point, Eq. (7) can be reduced to the phase map

$$e^{i\theta_{n+1}(\boldsymbol{r})} = \mathcal{L} e^{i\theta_n(\boldsymbol{r})} / |\mathcal{L} e^{i\theta_n(\boldsymbol{r})}|^{1+ic_2}. \tag{8}$$

First, we carry out the linear stability analysis of plane wave solutions of the CGLM

$$\hat{\psi}_n(\boldsymbol{r}) = e^{-|\boldsymbol{q}|^2} \exp[i\{\boldsymbol{q}\cdot\boldsymbol{r} - (c_1 - c_2)|\boldsymbol{q}|^2 n\}], \tag{9}$$

with a constant vector $\boldsymbol{q}$. Because the solutions have no phase singular point ($\hat{\psi}_n \neq 0$), we use the phase map (8), in which the plane wave solutions can be written in the form $\hat{\theta}_n(\boldsymbol{r}) = \boldsymbol{q}\cdot\boldsymbol{r} - (c_1 - c_2)|\boldsymbol{q}|^2 n + \text{const}$. By substituting $\theta_n = \hat{\theta}_n + \Delta_n$ into Eq. (8), the linearized equation for Δ_n is obtained as $\Delta_{n+1}(\boldsymbol{r}) = \Re[(1 - ic_2) e^{(1+ic_1)(\nabla^2 + 2i\boldsymbol{q}\cdot\nabla)} \Delta_n(\boldsymbol{r})]$. Therefore, the Fourier transform $\tilde{\Delta}_n(\boldsymbol{k})$ of Δ_n obeys

$$\tilde{\Delta}_{n+1}(\boldsymbol{k}) = e^{\Lambda_q(\boldsymbol{k})} \tilde{\Delta}_n(\boldsymbol{k}), \tag{10}$$

where $\Lambda_{\boldsymbol{q}}(\boldsymbol{k}) = -|\boldsymbol{k}|^2 - 2ic_1\boldsymbol{q}\cdot\boldsymbol{k} + \ln\{[(1 + ic_2)/2] \times e^{ic_1|\boldsymbol{k}|^2 + 2\boldsymbol{q}\cdot\boldsymbol{k}} + [(1 - ic_2)/2] e^{-ic_1|\boldsymbol{k}|^2 - 2\boldsymbol{q}\cdot\boldsymbol{k}}\}$. If $\Re\{\Lambda_{\boldsymbol{q}}(\boldsymbol{k})\} > 0$, the plane wave with the wave number $\boldsymbol{q}$ is linearly unstable against the perturbation with a wave number $\boldsymbol{k}$. Expansion of $\Lambda_{\boldsymbol{q}}(\boldsymbol{k})$ to fourth order in $|\boldsymbol{k}|$ leads to

$$\Lambda_{\boldsymbol{q}}(\boldsymbol{k}) \approx -iV_g|\boldsymbol{k}| - D_2|\boldsymbol{k}|^2 + i\Omega_g|\boldsymbol{k}|^3 - D_4|\boldsymbol{k}|^4, \tag{11}$$

with $V_g = 2(c_1 - c_2)q_{\boldsymbol{k}}$, $D_2 = 1 + c_1c_2 - 2(1 + c_2^2)q_{\boldsymbol{k}}^2$, $\Omega_g = \frac{2}{3}(1 + c_2^2)(3c_1 - 4c_2 q_{\boldsymbol{k}}^2) q_{\boldsymbol{k}}$, and $D_4 = \frac{1}{6}(1 + c_2^2) \times \{3c_1^2 - 24c_1c_2 q_{\boldsymbol{k}}^2 + 8(1 + 3c_2^2) q_{\boldsymbol{k}}^4\}$. Here $q_{\boldsymbol{k}} = \boldsymbol{q}\cdot\boldsymbol{k}/|\boldsymbol{k}|$. In the case that $D_2 < 0$, that is, the wave number $\boldsymbol{q}$ satisfies $|\boldsymbol{q}|^2 > q_E^2 \equiv (1 + c_1c_2)/2(1 + c_2^2)$, the plane wave solution is linearly unstable against long-wavelength perturbations. This instability is identical to the Eckhaus instability observed in the CGLE [4]. In particular, the spatially uniform state loses its stability at $1 + c_1c_2 = 0$, which is the same as the Benjamin-Feir-Newell criterion in the CGLE, and the Benjamin-Feir instability occurs for $1 + c_1c_2 < 0$. Then $D_2 < 0$ is satisfied for arbitrary wave numbers, and thus all plane wave solutions are linearly unstable. It is expected that the absolute instability of the plane wave solutions [14] can be also investigated.

Next, we show numerical results of the CGLM in a 2D system with the linear size $L = 128\pi$. We have numerically confirmed that Eq. (7) exhibits the same behavior as that in Eq. (6). Numerical cost to solve Eq. (6) is almost the same as that for Eq. (7), and z_n can be obtained from ψ_n but not vice versa. Therefore, we use Eq. (6) instead of Eq. (7) for the numerical simulations.

Slightly below the critical point $1 + c_1c_2 = 0$ of the Benjamin-Feir instability, the phase turbulence arises from initial conditions $\psi_n \approx 1$. As shown in Fig. 1(a), the amplitude $|\psi_n|$ has the cellular structure as well as in the CGLE [15]. The phases $\arg\psi_n$ and θ_n have the spatial structure similar to that of the amplitude, and its spatial mean slowly increases.

Now we prove that the phase turbulence observed in the CGLM coincides with that in the CGLE. Because this turbulence has no phase singular point, we can use the phase map (8) in this proof. As shown in the linear stability analysis given above, only the long-wavelength modes are destabilized slightly below the critical point $1 + c_1c_2 = 0$. Therefore, the spatial scale of the variation of the phase variable θ_n is expected to be large near the critical point. By letting the spatial scale be of order $\delta^{-1/2}$ with a smallness parameter δ, the term $\nabla^2 e^{i\theta_n}$ is estimated to be of order δ, and the linear operator $\mathcal{L}$ is expanded as $\mathcal{L} = e^{(1+ic_1)\nabla^2} \approx 1 + (1 + ic_1)\nabla^2 + \frac{1}{2}(1 + ic_1)^2\nabla^2\nabla^2 + \mathcal{O}(\delta^3)$. Substituting this expansion into Eq. (8) and setting $\theta_{n+1} - \theta_n \to \partial\theta_n/\partial n$, we obtain the Kuramoto-Sivashinsky (KS) equation:

$$\frac{\partial\theta_n}{\partial n} = (1 + c_1c_2)\nabla^2\theta_n + (c_2 - c_1)(\nabla\theta_n)^2 - \frac{1}{2}(c_1^2 - 2c_1c_2 - 1)\nabla^2\nabla^2\theta_n. \tag{12}$$

It should be noted that the coefficients of $\nabla^2\theta_n$ and $(\nabla\theta_n)^2$ in Eq. (12) coincide with those in the KS equation derived

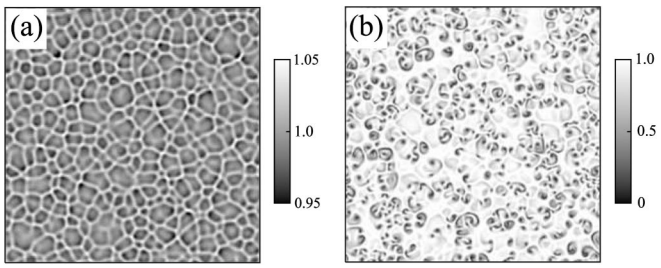

FIG. 1. Snapshots of $|\psi_n|$ of (a) phase turbulence for $(c_1, c_2) = (-1, 1.2)$ and (b) amplitude turbulence for $(c_1, c_2) = (-1, 0.6)$. In (b), there are 544 defects.

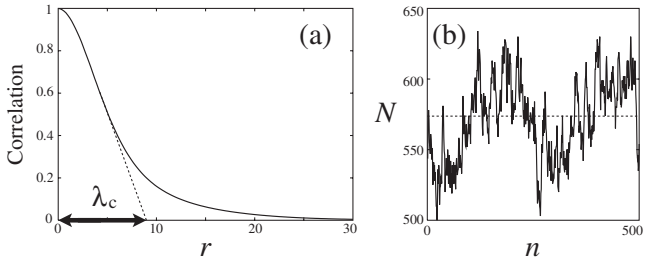

FIG. 2. Statistics of amplitude turbulence for $(c_1, c_2) = (-1, 0.6)$. (a) Spatial correlation $\Re\langle\psi_n(\boldsymbol{r})\psi_n^*(\boldsymbol{0})\rangle/\langle|\psi_n(\boldsymbol{0})|^2\rangle$, where $\langle\cdot\rangle$ denotes time averaging. The correlation length λ_c is defined in the same way as that in Ref. [17]. (b) Temporal evolution of the number N of defects in the whole space. The dashed line indicates the average number $\langle N\rangle \approx 572.9$.

from the CGLE by the phase reduction method, while the coefficients of $\nabla^2\nabla^2\theta_n$ derived from the CGLM and the CGLE are different [2,16]. This deviation may be carried by the difference of the definitions of the "phases," θ_n for the CGLM and $\arg\psi$ for the CGLE. Note that the deviation vanishes at the critical point $1 + c_1c_2 = 0$ and that, in the limit $1 + c_1c_2 \to 0$, the amplitude fluctuation vanishes ($|\psi_n| \to 1$), and thus θ_n approaches $\arg\psi_n$. These facts imply that the phase turbulences in the CGLM and the CGLE are quantitatively the same near the critical point. One may find that the coefficient of $\nabla^2\nabla^2\theta_n$ is different from D_4 in Eq. (11) for $\boldsymbol{q} = \boldsymbol{0}$. This is because the growth rate of Eq. (10), $\tilde{\Delta}_{n+1} - \tilde{\Delta}_n = (e^{\Lambda_q} - 1)\tilde{\Delta}_n$, is not $\Lambda_{\boldsymbol{q}}(\boldsymbol{k})$ but $[e^{\Lambda_q(\boldsymbol{k})} - 1]$, whose long-wavelength expansion for $\boldsymbol{q} = \boldsymbol{0}$ gives the coefficients of Eq. (12).

In addition to the phase turbulence, we observe the amplitude turbulence for $(c_1, c_2) = (-1, 0.6)$ [Fig. 1(b)], which is characterized by the exponential decay of the spatial correlation [Fig. 2(a)]. In this state, a lot of phase singular points (defects) exist over the whole space. The temporal evolution of the number N of defects [Fig. 2(b)] shows that pairs of defects are created and annihilate in time. We find that the correlation length λ_c defined in Fig. 2(a) is approximately equal to the mean distance d_m between a defect and its nearest neighbor: $\lambda_c \approx d_m \approx 9.0$. Because the defect turbulence observed in the CGLE also has these characteristics [17], the amplitude turbulence in the CGLM is expected to be identical to the defect turbulence in the CGLE.

For $(c_1, c_2) = (-1.0, 0.4)$, after the transient amplitude turbulent state, spiral waves tend to appear and eventually cover the whole space. The amplitude shows no temporal evolution, as shown in Fig. 3(a), while the phase exhibits the spiral waves, which rotate at a constant speed. This state is called either the frozen state (FS) or the vortex glass state [9]. For $(c_1, c_2) = (-3.0, 0.4)$, although spiral waves also occur, the amplitude is not frozen, and both the phase and the amplitude have spiral structures [Fig. 3(b)]. Hereafter we call this state the amplitude spiral state (ASS).

Figure 4 depicts details of the spatial structures near the spiral core in the FS and the ASS. There are at least three

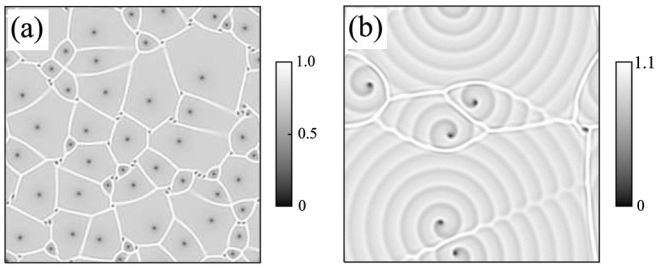

FIG. 3. Snapshots of $|\psi_n|$ of (a) the FS for $(c_1, c_2) = (-1, 0.4)$ and (b) the ASS for $(c_1, c_2) = (-3, 0.4)$.

qualitative differences between the FS and the ASS. First, the FS has an ordered spiral structure in the phase [Fig. 4(a)] and a rotationally symmetric hole structure in the amplitude [Fig. 4(b)]. However, the ASS has a distorted spiral in the phase [Fig. 4(c)] and an ordered spiral in the amplitude [Fig. 4(d)]. In the ASS case, the spiral structures in the amplitude and the phase have opposite rotational directions. Second, the position of the spiral core is motionless in the FS, while the core position rotates in the ASS. For example, the core in Fig. 4(d) rotates counterclockwise. Third, far from the spiral core, the FS exhibits the plane wave described by Eq. (9), while the ASS exhibits the plane wave with amplitude modulations. As shown below, the latter seems identical to the modulated amplitude wave (MAW) observed in the 1D CGLE, which is described as $\psi(x, t) = a(x - vt)e^{i(\nu x + \omega t)}$ [18,19]. In the 1D CGLM, we found a solution [Fig. 5(a)] satisfying the relation $\psi_n(x) = a(x - vn)e^{i(\nu x + \omega n)}$, which was demonstrated by the fact that $\psi_n(x)e^{-i(\nu x + \omega n)}$ exhibits the translational motion with keeping its profile [Fig. 5(b)]. The

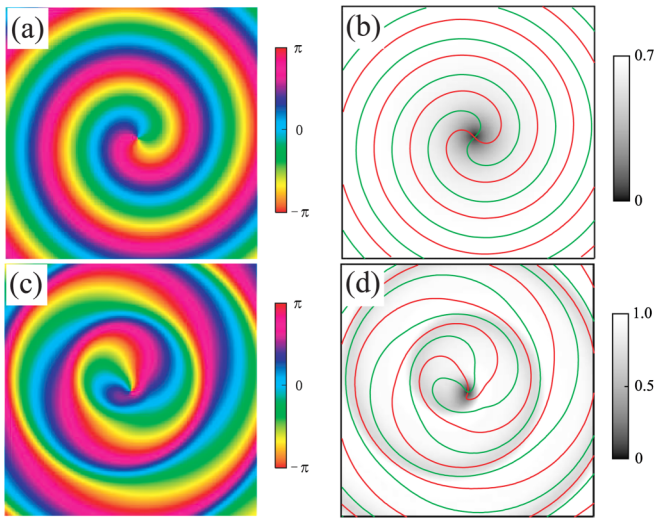

FIG. 4 (color online). Snapshots of (a),(b) the FS for $(c_1, c_2) = (-2, 0.4)$ in a subsystem of the linear size $l = 12.5\pi$ and (c),(d) the ASS for $(c_1, c_2) = (-3, 0.5)$ in a subsystem of the linear size $l = 31.25\pi$. (a),(c) Phase field $\arg\psi_n$; (b),(d) amplitude field $|\psi_n|$ with isophase curves (red: $\Re\psi_n = 0$; green: $\Im\psi_n = 0$).

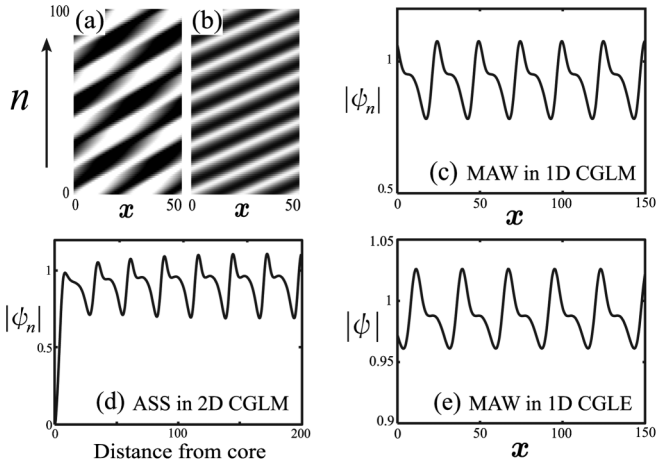

FIG. 5. Temporal evolutions of (a) $\Re[\psi_n(x)]$ and (b) $\Re[\psi_n(x)e^{-i(\nu x+\omega n)}]$ ($\nu = 0.125$, $\omega \approx 0.2504$) in the 1D CGLM. (c)–(e) Snapshots of the amplitude patterns. The parameter values of both the CGLM and the CGLE are $(c_1, c_2) = (-3, 0.5)$, and $D = 1.0$ for the CGLE.

amplitude pattern of this solution [Fig. 5(c)] is quite similar to those of the plane wave of the ASS [Fig. 5(d)] and the MAW in the 1D CGLE [Fig. 5(e)]. It should be noted that, depending on initial conditions, both the FS and the ASS can be observed (and, hence, both are stable) for parameter values in a certain range in the (c_1, c_2) space.

We found the ASS in the present Letter. In addition, we numerically obtained the ASS in the 2D CGLE (*not* the CGLM) from specific initial conditions [20]. Hence, the ASS is a stable state of the CGLE, and this fact implies that it is possible to observe the ASS in other oscillatory media. It was found that the long-wavelength modulated spiral can be observed in the CGLE with heterogeneity [21] and the Belousov-Zhabotinsky reaction [22] and that the CGLE with a constant term exhibits a state in which both the amplitude and the phase have spiral structures [23]. To investigate the relevance of these states with the ASS is a future problem.

The main difference between the CGLE and the CGLM is the presence or absence of the relaxation process to the limit-cycle attractor ($|\psi| = 1$). In spite of the difference, the results presented in this Letter reveal that the CGLM can well reproduce the dynamics observed in the CGLE. Therefore, we believe that the relaxation process does not play an important role in the CGLE and that the CGLE can be well described by only the phase dynamics appropriately constructed. These facts may give new insight into the understanding of oscillatory media.

We thank A. S. Mikhailov and N. Fujiwara for valuable comments. This study was partially supported by the 21st Century COE Program "Center of Excellence for Research and Education on Complex Functional Mechanical Systems" at Kyoto University.

*tsuka@acs.i.kyoto-u.ac.jp
†Deceased.

[1] M. C. Cross and P. C. Hohenberg, Rev. Mod. Phys. **65**, 851 (1993).
[2] Y. Kuramoto, *Chemical Oscillations, Waves, and Turbulence* (Springer-Verlag, Berlin, 1984); *Chemical Oscillations, Waves, and Turbulence* (Dover, New York, 2003).
[3] T. Bohr, M. H. Jensen, G. Paladin, and A. Vulpiani, *Dynamical Systems Approach to Turbulence* (Cambridge University Press, Cambridge, England, 1998).
[4] I. S. Aranson and L. Kramer, Rev. Mod. Phys. **74**, 99 (2002).
[5] H. Chaté and P. Manneville, Physica (Amsterdam) **224A**, 348 (1996).
[6] Y. Oono and S. Puri, Phys. Rev. Lett. **58**, 836 (1987).
[7] M.-N. Chee, R. Kapral, and S. G. Whittington, J. Chem. Phys. **92**, 7315 (1990).
[8] T. Bohr, A. W. Pedersen, M. H. Jensen, and D. Rand, in *New Trends in Nonlinear Dynamics and Pattern-Forming Phenomena*, edited by P. Coullet and P. Huerre (Plenum, New York, 1990); T. Bohr, A. W. Pedersen, and M. H. Jensen, Phys. Rev. A **42**, 3626 (1990).
[9] G. Huber, P. Alstrøm, and T. Bohr, Phys. Rev. Lett. **69**, 2380 (1992).
[10] X.-G. Wu and R. Kapral, J. Chem. Phys. **94**, 1411 (1991).
[11] A. Torcini, H. Frauenkron, and P. Grassberger, Phys. Rev. E **55**, 5073 (1997).
[12] S. Uchiyama and H. Fujisaka, Phys. Rev. E **56**, 99 (1997).
[13] T. Watanabe, Y. Tsubo, and H. Fujisaka, Phys. Rev. E **65**, 026213 (2002).
[14] I. S. Aranson, L. Aranson, L. Kramer, and A. Weber, Phys. Rev. A **46**, R2992 (1992).
[15] P. Manneville and H. Chaté, Physica (Amsterdam) **96D**, 30 (1996).
[16] N. Tsukamoto, H. Fujisaka, and K. Ouchi, Prog. Theor. Phys. **116**, 669 (2006).
[17] P. Coullet, L. Gil, and J. Lega, Phys. Rev. Lett. **62**, 1619 (1989).
[18] A. Torcini, Phys. Rev. Lett. **77**, 1047 (1996).
[19] L. Brusch, M. G. Zimmermann, M. van Hecke, M. Bär, and A. Torcini, Phys. Rev. Lett. **85**, 86 (2000).
[20] We observed the ASS in the 2D CGLE with the initial condition for the ψ field of the ASS obtained in the CGLM. The parameter values used in the numerical simulation of Eq. (1) are $c_1 = -3.0$, $c_2 = 0.5$, and $D = 1.0$. For these parameters, "usual" initial conditions lead to the FS.
[21] L. Brusch, A. Torcini, and M. Bär, Phys. Rev. Lett. **91**, 108302 (2003).
[22] L. Q. Zhou and Q. Ouyang, Phys. Rev. Lett. **85**, 1650 (2000).
[23] A. S. Mikhailov (private communication); N. Fujiwara, Ph.D. thesis, Kyoto University, 2007.